Published in final edited form as:
J Comput Assist Tomogr. 2013 ; 37(3): . doi:10.1097/RCT.0b013e318282d935.

Comparing primary tumors and metastatic nodes in head and neck cancer using intravoxel incoherent motion imaging: a preliminary experience

Yonggang Lu, Ph.D.[1], **Jacobus F.A. Jansen, Ph.D.**[2], **Hilda E. Stambuk, M.D.**[3], **Gaorav Gupta, M.D.**[4], **Nancy Lee, M.D.**[4], **Mithat Gonen, Ph.D.**[5], **Andre Moreira, M.D.**[6], **Yousef Mazaheri, Ph.D.**[1,3], **Snehal G. Patel, M.D.**[7], **Joseph O. Deasy, Ph.D.**[1], **Jatin P. Shah, M.D.**[7], and **Amita Shukla-Dave, Ph.D.**[1,3]

[1]Department of Medical Physics, Memorial Sloan-Kettering Cancer Center, New York, NY, USA. [2]Department of Radiology, Maastricht University Medical Center, Maastricht, The Netherlands. [3]Department of Radiology, Memorial Sloan-Kettering Cancer Center, New York, NY, USA. [4]Department of Radiation Oncology, Memorial Sloan-Kettering Cancer Center, New York, NY, USA. [5]Department of Biostatistics, Memorial Sloan-Kettering Cancer Center, New York, NY, USA. [6]Department of Pathology, Memorial Sloan-Kettering Cancer Center, New York, NY, USA. [7]Department of Surgery, Memorial Sloan-Kettering Cancer Center, New York, NY, USA.

Abstract

Objective—To use intravoxel incoherent motion (IVIM) imaging for investigating differences between primary head and neck tumors and nodal metastases and evaluating IVIM efficacy in predicting outcome.

Methods—Sixteen patients with HN cancer underwent IVIM DWI on a 1.5T MRI scanner. The significance of parametric difference between primary tumors and metastatic nodes were tested. Probabilities of progression-free survival (PFS) and overall survival (OS) were estimated using the Kaplan-Meier method.

Results—In comparison to metastatic nodes, the primary tumors had significantly higher vascular volume fraction (f) ($p<0.0009$), and lower diffusion coefficient (D) ($p<0.0002$). Patients with lower standard deviation for D had prolonged PFS and OS ($p<0.05$).

Conclusion—Pretreatment IVIM measures were feasible in investigating the physiological differences between the two tumor tissues. After appropriate validation, these findings might be useful in optimizing treatment planning and improving patient care.

Keywords

Intravoxel incoherent motion imaging (IVIM); head and neck (HN) cancer; primary tumor; metastatic neck node

Corresponding author: Amita Shukla-Dave Ph.D. Department of Medical Physics and Radiology Memorial Sloan-Kettering Cancer Center 1275 York Avenue, New York, New York 10065 Telephone: 212.639.3184 Fax: 212.717.3010 davea@mskcc.org.

All authors have no conflicts of interest with regard to this manuscript.

INTRODUCTION

Primary tumors in the head and neck have a strong tendency to invade loco-regional nodes[1-3]. The presence of neck nodal metastases often indicates the first step of disease progression from a more local and contained stage to a more aggressive stage. The key tumor-based prognostic factors for locoregional control of head and neck cancers include the presence and extent of nodal metastases, T-stage, and human papilloma virus (HPV) tumor positivity [2, 4-7]. Comparative imaging studies of primary tumors and metastatic neck nodes may reflect key physiological differences that underlie the important transition of the disease. The quantitative parameters measured by imaging may help optimize treatment planning strategies and thereby improve patient outcome in head and neck cancers.

Magnetic resonance imaging (MRI) is a non-invasive method that provides images of high spatial resolution with excellent tissue contrast and has shown promise in the detection, staging, prognosis and monitoring of head and neck cancers[8, 9]. However, on anatomical MRI images, primary tumors and metastatic neck nodes often exhibit similar signal intensities, indicating the weakness of anatomical MRI in accurately characterizing these two tumor tissues. Functional MRI techniques such as diffusion-weighted imaging (DWI) allow non-invasive measurement of water molecule diffusivity and have shown promise in the advanced quantification of tumor tissues[10, 11]. Prior head and neck cancer studies have shown that the apparent diffusion coefficient (ADC) derived from monoexponential modeling of the DWI data helps to enhance sensitivity and specificity in tumor differentiation[12-14], staging[15] and treatment response evaluation[16]. More recently, bi-exponential modeling such as intravoxel incoherent motion (IVIM) model derived from multiple b value DWI data (b is the gradient factor attenuation (s/mm^2)), has been found to provide simultaneously quantitative parameters that reflect diffusion and perfusion without the need for injection of a contrast agent[17, 18]. IVIM model regards biological tissue as two compartments of intravascular and extravascular spaces. By appropriate modeling, the characteristics of each compartment in biological tissues can be quantified. IVIM model was applied early in the investigation of diseases such as chronic brain ischemia [19], liver cirrhosis [20], and muscle inflammatory myopathy [21]. The use of IVIM has been expanded to characterize tumor biology and has shown its superiority over DWI in the detection and differentiation of prostate, pancreas and breast tumors[22-24]. The purpose of the present study was to apply IVIM model to simultaneously quantify the perfusion and diffusion measures in primary tumors and neck nodal metastases and investigate the physiological differences between these two tumor tissues. Additionally, pretreatment IVIM measures were evaluated for their efficacy in predicting patient outcome in head and neck cancers.

MATERIALS AND METHODS

Patients

Our institutional review board approved and issued a waiver of informed consent for this retrospective study, which was compliant with the Health Insurance Portability and Accountability Act. Inclusion criteria for the study were as follows: biopsy-proven head and neck squamous cell carcinoma (HNSCC) and presence of nodal metastasis in the neck. Between June 2010 and May 2011, 16 head and neck cancer patients (age: 38-64 years; M/F: 15/1; primary cancer: 11 oropharynx, 4 oral cavity and 1 nasopharynx; tumor size: 744-19,949 mm^3) were enrolled (Table 1). Each patient had a known primary tumor and regional metastatic node. Patients were treated with surgery (N=2) or chemo-radiation therapy (N=14).

IVIM

Pretreatment clinical MRI examinations were performed on a GE 1.5T Excite scanner (General Electric, Milwaukee, WI) with an 8-channel neurovascular phased-array coil. IVIM diffusion weighted imaging (DWI) was performed after standard multi-planar (sagittal, axial, and coronal) T1- and T2- weighted imaging.

IVIM images was acquired using a single-shot echo planar imaging (SS-EPI) spin echo sequence with 17 b values as derived from the geometric form b = (0, 10a, $10a^2$, ... , $10a^n$; a = 1.32, n = 16) [25]. The b values were as follows: b = 0, 13, 17, 23, 30, 40, 53, 70, 92, 122, 161, 212, 280, 369, 488, 644, and 850 s/mm^2, respectively. Other parameters were as follows: TR (repetition time) = 4000 ms, TE (echo time) = 90~104 ms, NEX (number of excitation) = 4, matrix = 128 × 128, FOV (field of view) = 20~22 cm, slices = 4~6, slice thickness = 6-8 mm. ASSET (array spatial sensitivity encoding technique) was turned off. Before IVIM scanning, a reference scan was used to reduce the Nyquist (N/2) ghosting artifacts. Images were all obtained in axial planes. To save acquisition time, diffusion encoding was performed along one direction [0.577, 0.577, 0.577], assuming that diffusion in tumors is isotropic. The total acquisition time for obtaining the IVIM data was approximately 4 minutes.

IVIM images were analyzed using the mono-exponential (equation 1) and bi-exponential (equation 2) models:

$$A_1 = S_0 \exp(-bADC) \quad [1]$$

$$A_2 = S_0 \left((1-f)\exp(-bD) + f\exp(-bD^*)\right) \quad [2]$$

where A_1 or A_2 and S_0 are the signal intensities with and without diffusion weighting respectively; b is the gradient factor (s/mm^2); ADC is the apparent diffusion coefficient (mm^2/s); f is the vascular volume fraction; D is the pure diffusion coefficient (mm^2/s); and D* is the pseudo-diffusion coefficient (mm^2/s) associated with blood perfusion [23, 24].

Since IVIM images are inherently noisy because of thermal or physiological factors, the signal intensity of a noisy IVIM image is given by:

$$S = A_i + n \quad [3]$$

where n is the noise intensity; and i = 1, 2 for the equation 1 and 2 respectively. The signals of S and n are Rician-distributed on the IVIM images [26].

To estimate the parameters, a chi-square cost function (χ^2) was defined and minimized [27]:

$$\chi^2(p) = \sum_{k=1}^{N_b} \frac{[M_k - MN(S_k(b_k, p))]^2}{\sigma^2} \quad [4]$$

where p is the estimated measure set; N_b is the number of b values (N_b =16 in this study); M_k is the signal intensity measured at the *kth* b value; σ is the standard deviation of noise; and $MN(S_k)$ is the averaged intensity calculated from the signals with Rician distribution. $MN(S_k)$ is given by[28, 29] :

$$MN\left(S^2\right) = {A_i}^2 + \frac{2N\sigma^2}{N_{avg}} \quad [5]$$

where N is the number of receiver channels (N = 8) and N_{avg} is the average number of IVIM data acquisition (N_{avg} = 4).

To estimate standard deviation of noise (σ) and signal-to-noise ratio (SNR) in the IVIM images acquired with the 8-channel phased-array coil, a region of interest (ROI)-based method that accounts for a multiple-channel MRI system with Rician-distributed noise and signal averaging was applied [28, 29]. The standard deviation of noise was estimated from a noise ROI that was positioned on the background of the image without signal (the yellow box in Figure 1), which was calculated as:

$$\sigma = \sqrt{\frac{N_{avg}}{2NL}\sum_{i=1}^{L} n_i^2} \quad [6]$$

where n is the noise intensity of each voxel and L is the number of voxels within the noise ROI.

The nonlinear least-square fitting method was performed to estimate the parameters. The subspace trust region algorithm, which is built into Matlab by the manufacturer, was used for the optimization procedure in the data fittings [30]. The parameters of each voxel were calculated. A multiple start scheme (10 times in this study) was used in the optimization procedure. For each time, the start value of each parameter was the random value chosen between the lower and upper bound of the measure set ($f \in (0, 1)$, $D \in (0, 4\times10\text{-}3\ mm^2/s)$, $D^* \in (0, 300\times10\text{-}3\ mm^2/s)$, $S_0 \in (0, 1000)$). With these multiple starts, the final estimated measure value was chosen as the estimated measure set with minimum chi-square (χ^2).

The location of primary tumors and metastatic nodes in 16 head and neck cancer patients was identified and manually segmented on standard MRI and DWI images by a neuroradiologist with more than 10 years of experience. For each patient, the total tumor volume was obtained by summing the voxel volume for all slices that contained tumor on T1 weighted images[13]. ROIs for IVIM fitting were prescribed on primary tumors and metastatic nodes on DWI images (b=0), avoiding necrotic areas. The data was fitted on a voxel-by-voxel basis and the derived measures were then averaged to yield mean and standard deviation (std) for ROI analysis The standard deviation of the measures describes the width of the distribution and is thought to be indicative of the heterogeneity in tumor tissues[31].

Patient assessment

Clinical assessment to evaluate outcome was done by a radiation oncologist with more than ten years of experience, incorporating clinical evaluation and imaging information obtained from PET/CT and MRI studies. Data was censored at the time of last follow-up. Tumor recurrence was classified on a scale of 0 to 3; where 0= no metastasis, 1= local or regional metastases, 2= distant metastases, 3= regional and distant metastases. Patient status was regarded as alive (score 0) and deceased (score 1). The primary end points calculated were progression-free survival (PFS) and overall survival (OS), consistent with published literature[32].

Statistical analysis

The Lilliefors test was used to test the normality of all IVIM derived measures from 16 head and neck cancer patients. Paired Student t-tests were performed to compare the difference in IVIM derived measures between 16 pairs of a primary tumor and a metastatic node. Non-parametric Spearman correlation coefficients (ρ) were calculated to investigate the correlation of the derived measures between the paired primary tumor and metastatic node. Parametric differences were tested using the statistical method of analysis of variance

(ANOVA). A p value of less than 0.05 indicated statistical significance. Univariate receiver operating characteristic (ROC) analyses were performed on the measures that were significantly different in the two groups. Multivariate ROC analyses were also performed on the combination of significant measures. For ROC analyses, the probabilities of estimated measures were first calculated with logistic regression models and then used for the construction of the ROC curves. Area under the ROC curves (AUC) for different measures were calculated to determine the accuracy of discrimination.

Measures derived from IVIM modeling for each pair of primary tumor and metastatic node, and the difference of these measures between paired primary tumor and metastatic node were used for the associations with clinical outcomes (OS and PFS). The Kaplan-Meier method was used to estimate the probabilities of survival in OS and PFS, and the log-rank test was performed to determine the measures that can classify patients into two groups with significant survival difference.

All programs for the above analyses were developed in-house using the software written in Matlab 6.5. The software was run on Windows system installed on a desktop workstation with Intel Pentium 4 CPU 3.20GHz and 3.24 GB RAM. The most computer-intensive program was voxelwise IVIM fitting. For example, the computational time for IVIM fitting of a ROI with 500 voxels was approximately 2 minutes.

RESULTS

The analysis was performed on pretreatment IVIM data acquired from 16 patients with paired primary tumors and metastatic nodes. Figure 1 shows the IVIM images and model fitting plots from two representative patients, having nodes with and without necrosis, respectively. For both patients' IVIM data, the biexponential function has a better fitting than the monoexponential function. For example, in the primary tumor of the first representative patient (Figure 1a and 1b), the biexponential fitting has a higher value of coefficient of determination (R^2) than the monoexponential fitting (0.96 vs 0.93). It can be observed that the fitted curves for primary tumors have different shapes from those for metastatic neck nodes; at high b values, the curve slopes from primary tumors are much lower than those for metastatic neck nodes, showing low diffusivity in the primary tumors. IVIM data obtained from the 16 head and neck cancer patients showed that the biexponential function had a significantly better fitting than the monoexponential function (for primary tumors, R^2=0.95±0.03 vs 0.85±0.10, p<0.0004; for metastatic nodes, R^2=0.98±0.02 vs 0.94±0.05, p<0.0009).

Normality test revealed that all IVIM derived measures appeared to have normal distribution (p<0.05). It was found that the ADC derived from the monoexponential model was not significantly different between the groups of primary tumors and metastatic nodes (p > 0.05; Table 2). However, the D value, derived from the bi-exponential model, was significantly lower (p=0.0002; Table 2; Figure 2) in primary tumors when compared with metastatic nodes. The perfusion-related measure f was also significant in comparing these two tumor tissues (p=0.0002; Table 2; Figure 2). It was found that there was significant correlation of all measures derived from IVIM (ADC, f, D and D*) between primary tumors and metastatic nodes (ρ ranged from 0.60 to 0.71; p values < 0.013; Table 2).

From the ROC curve analysis, the following measures were found to be significant: f (AUC = 0.71; p <0.008), and D (AUC=0.74; p< 0.003). Comparatively, ADC and D* were not significant [(AUC = 0.55; p< 0.29) for ADC, and (AUC = 0.53; p< 0.35) for D*]. The combination of f and D had the maximum AUC of 0.76, with a sensitivity of 62.5% and specificity of 81.25% (Table 3; Figure 3).

For clinical outcomes, 12 patients had no tumor recurrence, 1 patient had local or regional metastases, 2 patients had distant metastases, and 1 patient had regional and distant metastases; 1 patient was deceased and 15 patients were alive. The analysis by the Kaplan-Meier method showed that patients with lower standard deviation of diffusion coefficient (std(D)) from both primary tumors and metastatic nodes had prolonged PFS ($p<0.001$ for primary tumor; $p=0.017$ for metastatic node) and OS ($p=0.037$ for primary tumor; $p=0.037$ for metastatic node). Figure 4 displays the PFS curves for std(D) from primary tumors and metastatic nodes. There was no significance achieved when the difference of these measures between paired primary tumor and metastatic node were used for the associations with clinical outcomes ($p>0.05$).

DISCUSSION

In head and neck cancers, primary tumors often metastasize to loco-regional lymph nodes. Metastatic tumors invariably represent more aggressive tumors that may respond poorly to treatment[33, 34]. Accurate characterization of primary tumors and neck nodal metastases by non-invasive methods is important to help guide individualized treatment planning and improve cancer patient management. Therefore, it is clinically pertinent to study the physiological differences in primary and metastatic neck nodes, and evaluate their values in predicting outcome in head and neck cancer patients. Previous studies have investigated either primary tumors or metastatic nodes[12-16]. No study has been reported that compares these two tumor tissues. Our study is the first in proposing such an investigation using IVIM technique. The results of our study demonstrate that primary tumors have distinct *in vivo* MR signatures with significantly higher vascular fractions (f), and lower diffusion coefficients (D) than those in metastatic nodes in head and neck cancer. Additionally, this study also revealed that std i.e. width of the distribution of measure D (std(D)) was the most significant in predicting progression-free survival and overall survival.

The basic biological premise for the use of DWI in cancer is that malignant tissues are generally more cellular and vascular than normal tissues. There are several microscopic organizational features that affect tissue water diffusivity, tissue perfusion, cell density, distribution of cell sizes within a tissue, integrity of cellular membranes, and tissue organization[35]. Inverse correlation between the diffusion coefficient and cell density has been found in gliomas, prostate cancers and a few childhood tumors[1, 36, 37]. The novelty of IVIM is that it can characterize tumor diffusion more accurately than DWI, and provide an additional perfusion-related measure without injection of any contrast agent. The ADC value derived from the monoexponential model is a composite parameter that has the integrated effect of both diffusion and perfusion. Due to its composite effect, ADC value failed in distinguishing the primary tumor and metastatic node in this study (1.05 ± 0.31 vs $1.10\pm0.26*10^{-3}$ m^2/s; $p<0.38$). The IVIM technique has the potential to separate diffusion and perfusion and provide measures to quantify these two processes simultaneously. High-fold magnification of p values of D ($p<0.002$) and f ($p<0.0009$) clearly show that the primary tumors have diffusion and perfusion characteristics that are distinct from those of the metastatic nodes. These findings were further verified in the results of ROC analysis, which showed that the ADC was unsuccessful while f and D succeeded in differentiating the two tumor tissues. Of note, the combination of f and D was found to be the most significant in the differentiation study.

These physiological differences in diffusion and perfusion measures may play an important role in assessing early response to anti-angiogenic agents and in treatment planning where radiation dose de-escalation at the nodal site is being considered for HPV positive patients who have better outcome than HPV negative patients when treated with chemo-radiation

therapy. In future, different doses maybe given to the primary and nodal metastases in an attempt to lower toxicity while maintaining same outcome.

The link between DWI findings and angiogenesis is not direct[38-40]. It has been hypothesized by Koh et al that tumors with a higher pre-treatment ADC are more susceptible to the effects of therapy with vascular disrupting or anti-angiogenesis agents[41]. They suggested based on results of DWI in 15 patients with solid tumors (mostly colorectal and ovarian), that immature tumor vessels which predominate at the edge of necrotic regions (with high ADC values) are more susceptible to the anti-angiogenic agent bevacizumab.

The preliminary analysis of outcome results showed that the std(D) in both primary tumors and metastatic nodes was significant in predicting PFS and OS. It has been recently reported in a study with eighteen head and neck cancer patients undergoing induction chemotherapy that ADC may be a useful marker in predicting progression-free survival[42]. The same group had earlier reported that ADC can also be used as a marker for prediction and early detection of response to concurrent chemoradiation therapy in thirty three head and neck cancer patients[43]. Validation studies are needed to see if the above and our findings can be reproduced before making definitive conclusions about the prognostic nature of ADC or IVIM measures.

There are a few limitations in this study. First, it is a cross-sectional feasibility study that acquired and analyzed data from a small patient population (n=16) to assess the benefits of IVIM in investigating the difference between primary tumors and metastatic neck nodes. A large, prospective study is still warranted to validate the findings of the present study. Second, performance of the IVIM model was limited by the signal-to-noise ratio (SNR) at 1.5T. The SNRs of IVIM images obtained from 16 head and neck cancer patients in this study were in the range of 4 to 17 and the average SNR was 11. SNR can be increased by increasing the voxel size of the DW-MR image, number of excitation, or magnetic field strength (≥3 T). Finally, the exact nature of IVIM modeling still needs to be elucidated and a comparison to dynamic contrast enhanced MRI (MRI technique to assess microvasculature/perfusion in tumors) is warranted.

The present feasibility study shows interesting pretreatment results with IVIM data that can measure simultaneously diffusion and perfusion effects without the need to inject a contrast agent. Such pretreatment data may have translational applications in three areas: treatment planning, prediction of outcome, and monitoring treatment response. In the future, if pretreatment IVIM data can help distinguish tumors with a good prognosis from those with a poor prognosis, use of IVIM may allow individualized treatment planning for head and neck cancer patient. It may help identify patients at risk earlier so that they can be considered for treatment with antiangiogenic agents, hypoxia-targeting therapy, or gene therapy.

CONCLUSIONS

In conclusion, pretreatment IVIM is feasible in head and neck cancer patients with nodal metastases. All IVIM parameters between primary tumors and metastatic nodes were highly correlated; primary tumors had higher values of f and D. Measures of std(D) in both primary tumors and metastatic nodes were found to be predictors of outcome. After appropriate validation, these findings might be useful in optimizing treatment planning and improving patient care.

Acknowledgments

This study was conducted with support from National Cancer Institute/National Institutes of Health (grant number 1 R01 CA115895). The authors would like to thank the MRI technologists for their great efforts to help perform the

MRI examinations and Ms. Dara Srisaranard for her helpful contribution to patient enrollment and data management. We thank Ms Sandhya George for editing the manuscript.

ABBREVIATION KEY

ADC	Apparent Diffusion Coefficient
DWI	Diffusion Weighted Imaging
FOV	Field Of View
HNSCC	Head and Neck Squamous Cell Carcinoma
IVIM	Intravoxel Incoherent Motion Imaging
MRI	Magnetic Resonance Imaging
NEX	Number of Excitation
OS	Overall Survival
PFS	Progression-Free Survival
ROC	Receiver Operating Characteristic
ROI	Region Of Interest
SS-EPI	Single Shot Echo Planar Imaging
TR	Repetition Time
TE	Echo Time

REFERENCES

1. Forastiere AA, Trotti A, Pfister DG, et al. Head and neck cancer: recent advances and new standards of care. J Clin Oncol. 2006; 24:2603–5. [PubMed: 16763271]
2. Awada A, de Castro G Jr. Head and neck cancer emerging strategies: advances and new challenges. Curr Opin Oncol. 2009; 21:191–3. [PubMed: 19346942]
3. Stambuk HE, Karimi S, Lee N, et al. Oral cavity and oropharynx tumors. Radiologic Clinics of North America. 2007; 45:1–20. [PubMed: 17157621]
4. Snow GB, van den Brekel MW, Leemans CR, et al. Surgical management of cervical lymph nodes in patients with oral and oropharyngeal cancer. Recent Results Cancer Res. 1994; 134:43–55. [PubMed: 8153441]
5. Baatenburg de Jong RJ, Hermans J, Molenaar J, et al. Prediction of survival in patients with head and neck cancer. Head Neck. 2001; 23:718–24. [PubMed: 11505480]
6. Mukherji SK, O'Brien SM, Gerstle RJ, et al. Tumor volume: an independent predictor of outcome for laryngeal cancer. J Comput Assist Tomogr. 1999; 23:50–4. [PubMed: 10050807]
7. Rudat V, Dietz A, Schramm O, et al. Prognostic impact of total tumor volume and hemoglobin concentration on the outcome of patients with advanced head and neck cancer after concomitant boost radiochemotherapy. Radiother Oncol. 1999; 53:119–25. [PubMed: 10665788]
8. Shah GV, Wesolowski JR, Ansari SA, et al. New directions in head and neck imaging. J Surg Oncol. 2008; 97:644–8. [PubMed: 18493943]
9. de Bree R, Castelijns JA, Hoekstra OS, et al. Advances in imaging in the work-up of head and neck cancer patients. Oral Oncol. 2009; 45:930–5. [PubMed: 19692289]
10. Chawla S, Kim S, Wang S, et al. Diffusion-weighted imaging in head and neck cancers. Future Oncol. 2009; 5:959–75. [PubMed: 19792966]
11. Padhani AR. Diffusion magnetic resonance imaging in cancer patient management. Semin Radiat Oncol. 2011; 21:119–40. [PubMed: 21356480]

12. Sumi M, Sakihama N, Sumi T, et al. Discrimination of metastatic cervical lymph nodes with diffusion-weighted MR imaging in patients with head and neck cancer. AJNR Am J Neuroradiol. 2003; 24:1627–34. [PubMed: 13679283]
13. Koc O, Paksoy Y, Erayman I, et al. Role of diffusion weighted MR in the discrimination diagnosis of the cystic and/or necrotic head and neck lesions. Eur J Radiol. 2007; 62:205–13. [PubMed: 17188444]
14. Jansen JF, Stambuk HE, Koutcher JA, et al. Non-gaussian analysis of diffusion-weighted MR imaging in head and neck squamous cell carcinoma: A feasibility study. AJNR Am J Neuroradiol. 2010; 31:741–8. [PubMed: 20037133]
15. Vandecaveye V, De Keyzer F, Nuyts S, et al. Detection of head and neck squamous cell carcinoma with diffusion weighted MRI after (chemo)radiotherapy: correlation between radiologic and histopathologic findings. Int J Radiat Oncol Biol Phys. 2007; 67:960–71. [PubMed: 17141979]
16. Kato H, Kanematsu M, Tanaka O, et al. Head and neck squamous cell carcinoma: usefulness of diffusion-weighted MR imaging in the prediction of a neoadjuvant therapeutic effect. Eur Radiol. 2009; 19:103–9. [PubMed: 18641991]
17. Le Bihan D, Breton E, Lallemand D, et al. Separation of diffusion and perfusion in intravoxel incoherent motion MR imaging. Radiology. 1988; 168:497–505. [PubMed: 3393671]
18. Le Bihan D. Intravoxel incoherent motion perfusion MR imaging: a wake-up call. Radiology. 2008; 249:748–52. [PubMed: 19011179]
19. Le Bihan D, Breton E, Lallemand D, et al. MR imaging of intravoxel incoherent motions: application to diffusion and perfusion in neurologic disorders. Radiology. 1986; 161:401–7. [PubMed: 3763909]
20. Luciani A, Vignaud A, Cavet M, et al. Liver Cirrhosis: Intravoxel Incoherent Motion MR Imaging-Pilot Study. Radiology. 2008; 249:891–899. [PubMed: 19011186]
21. Qi J, Olsen NJ, Price RR, et al. Diffusion-weighted imaging of inflammatory myopathies: polymyositis and dermatomyositis. J Magn Reson Imaging. 2008; 27:212–7. [PubMed: 18022843]
22. Riches SF, Hawtin K, Charles-Edwards EM, et al. Diffusion-weighted imaging of the prostate and rectal wall: comparison of biexponential and monoexponential modelled diffusion and associated perfusion coefficients. NMR Biomed. 2009; 22:318–25. [PubMed: 19009566]
23. Lemke A, Laun FB, Klau M, et al. Differentiation of pancreas carcinoma from healthy pancreatic tissue using multiple b-values: comparison of apparent diffusion coefficient and intravoxel incoherent motion derived parameters. Investigative Radiology. 2009; 44:769–75. [PubMed: 19838121]
24. Sigmund EE, Cho GY, Kim S, et al. Intravoxel incoherent motion imaging of tumor microenvironment in locally advanced breast cancer. Magn Reson Med. 2011; 65:1437–1447. [PubMed: 21287591]
25. Moore RJ, Issa B, Tokarczuk P, et al. In vivo intravoxel incoherent motion measurements in the human placenta using echo-planar imaging at 0.5 T. Magn Reson Med. 2000; 43:295–302. [PubMed: 10680695]
26. Gudbjartsson H, Patz S. The Rician distribution of noisy MRI data. Magn Reson Med. 1995; 34:910–4. [PubMed: 8598820]
27. Kristoffersen A. Statistical assessment of non-Gaussian diffusion models. Magn Reson Med. 2011; 66:1639–1648. [PubMed: 21523826]
28. Constantinides CD, Atalar E, McVeigh ER. Signal-to-noise measurements in magnitude images from NMR phased arrays. Magn Reson Med. 1997; 38:852–7. [PubMed: 9358462]
29. Kristoffersen A. Optimal estimation of the diffusion coefficient from non-averaged and averaged noisy magnitude data. J Magn Reson. 2007; 187:293–305. [PubMed: 17572124]
30. More JJ, Sorensen DC. Computing a Trust Region Step. Siam Journal on Scientific and Statistical Computing. 1983; 4:553–572.
31. Lee CH, Choi JW, Kim KA, et al. Usefulness of standard deviation on the histogram of ultrasound as a quantitative value for hepatic parenchymal echo texture; preliminary study. Ultrasound Med Biol. 2006; 32:1817–26. [PubMed: 17169693]
32. Posner MR, Hershock DM, Blajman CR, et al. Cisplatin and fluorouracil alone or with docetaxel in head and neck cancer. N Engl J Med. 2007; 357:1705–15. [PubMed: 17960013]

33. Cooper JS, Pajak TF, Forastiere AA, et al. Postoperative concurrent radiotherapy and chemotherapy for high-risk squamous-cell carcinoma of the head and neck. N Engl J Med. 2004; 350:1937–44. [PubMed: 15128893]
34. Bernier J, Domenge C, Ozsahin M, et al. Postoperative irradiation with or without concomitant chemotherapy for locally advanced head and neck cancer. N Engl J Med. 2004; 350:1945–52. [PubMed: 15128894]
35. Padhani AR, Koh DM. Diffusion MR imaging for monitoring of treatment response. Magn Reson Imaging Clin N Am. 2011; 19:181–209. [PubMed: 21129641]
36. Humphries PD, Sebire NJ, Siegel MJ, et al. Tumors in pediatric patients at diffusion-weighted MR imaging: apparent diffusion coefficient and tumor cellularity. Radiology. 2007; 245:848–54. [PubMed: 17951348]
37. Zelhof B, Pickles M, Liney G, et al. Correlation of diffusion-weighted magnetic resonance data with cellularity in prostate cancer. BJU Int. 2009; 103:883–8. [PubMed: 19007373]
38. Figueiras RG, Padhani AR, Goh VJ, et al. Novel oncologic drugs: what they do and how they affect images. Radiographics. 2011; 31:2059–91. [PubMed: 22084189]
39. Jansen JF, Koutcher JA, Shukla-Dave A. Non-invasive imaging of angiogenesis in head and neck squamous cell carcinoma. Angiogenesis. 2010; 13:149–60. [PubMed: 20383743]
40. Suh JY, Cho G, Song Y, et al. Is apparent diffusion coefficient reliable and accurate for monitoring effects of antiangiogenic treatment in a longitudinal study? J Magn Reson Imaging. 2012; 35:1430–6. [PubMed: 22314928]
41. Koh DM, Blackledge M, Collins DJ, et al. Reproducibility and changes in the apparent diffusion coefficients of solid tumours treated with combretastatin A4 phosphate and bevacizumab in a two-centre phase I clinical trial. Eur Radiol. 2009; 19:2728–38. [PubMed: 19547986]
42. Berrak S, Chawla S, Kim S, et al. Diffusion weighted imaging in predicting progression free survival in patients with squamous cell carcinomas of the head and neck treated with induction chemotherapy. Acad Radiol. 2011; 18:1225–32. [PubMed: 21835649]
43. Kim S, Loevner L, Quon H, et al. Diffusion-weighted magnetic resonance imaging for predicting and detecting early response to chemoradiation therapy of squamous cell carcinomas of the head and neck. Clin Cancer Res. 2009; 15:986–94. [PubMed: 19188170]

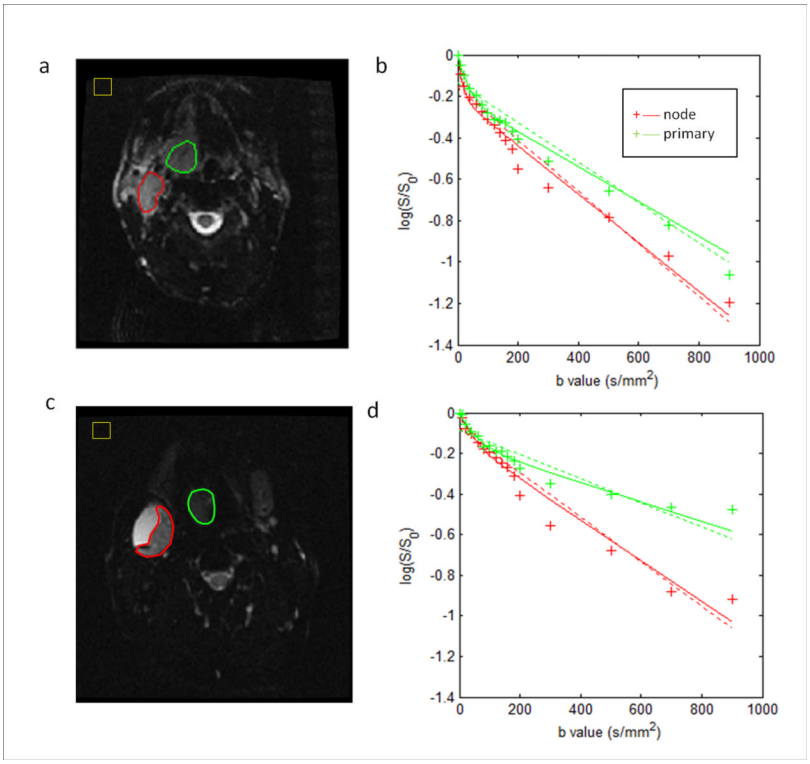

Figure 1.

IVIM images and model fits from two representative patients. (a) and (b) for a patient without necrotic node (male, 54 years old, oropharynx tumor); and (c) and (d) for a patient with necrotic node (male, 56 years old, oropharynx tumor). The primary tumors and metastatic nodes excluding necrotic areas (outlined as green and red, respectively) were prescribed on IVIM images at b=0 s/mm^2 in (a) and (c). IVIM model fits for the primary tumors and metastatic nodes are shown in (b) and (d). The solid curves represent the fits from the biexponential function and the dashed curves represent the fits from the monoexponential function. In (b) and (d), the vertical axis represents the logarithmic of the signal (S/S_0), and the horizontal axis represents the b values. In (a) and (c), the yellow boxes depict the noise ROIs for estimating image noise. Note: In the figure the primary tumors were labelled as primary and the metastatic nodes as node.

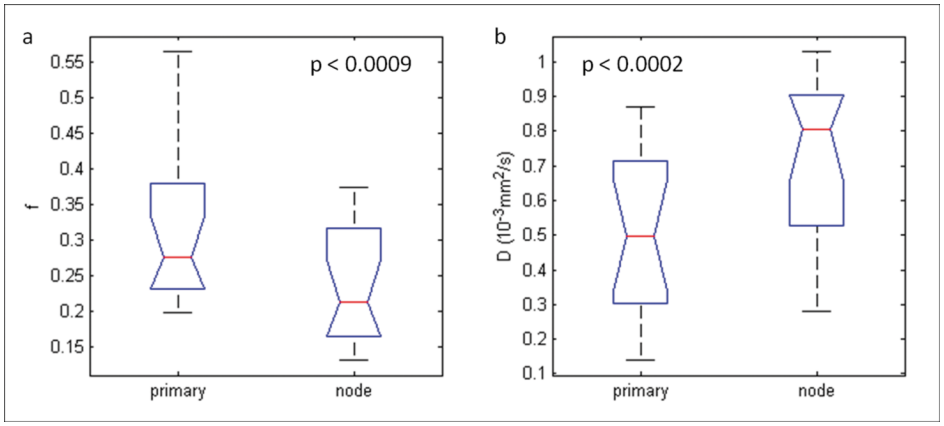

Figure 2.

Box-and-whisker plots illustrating parameter differences with statistical significance between the primary tumors and metastatic nodes in 16 patients. Note: In the figure the primary tumors were labelled as primary and the metastatic nodes as node.

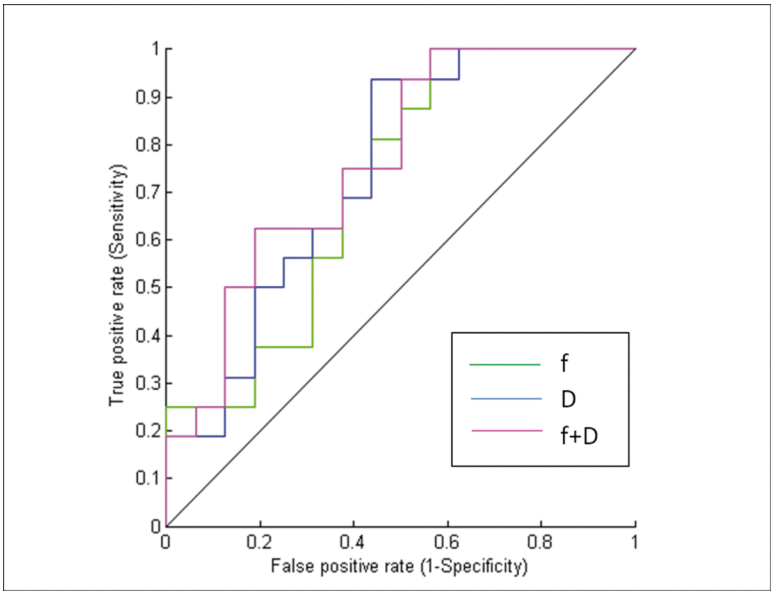

Figure 3.
ROC curves for differentiation of primary tumors from metastatic nodes based on the values of f, D and the combination of f and D.

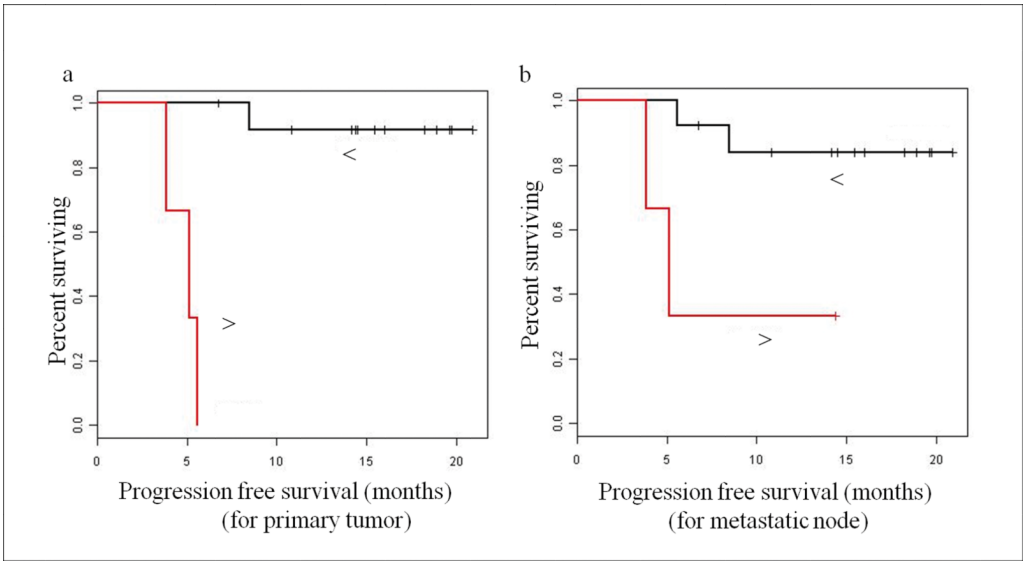

Figure 4.

Kaplan-Meier progression-free survival (PFS) plots: (a) Patients stratified at median std(D) of primary tumor, and (b) patients stratified at median std(D) of metastatic node. Note: In both Figure (a) and (b), red lines represent the plot with std(D) > median, and the black lines represent the plot with std(D) < median. The dots above each line represent censored observations.

Table 1

Patient characteristics

Characteristics	Value
Total patients	16
Demographics	
Mean age (y)	55
Age range (y)	38-64
Male/Female	15/1
Location of primary tumor	
Oropharynx	11
Oral cavity	4
Nasopharynx	1
Stages	
Stage III	1
Stage IV	15
Tumor size (mm^3)	744-19,949
Therapy types	
Surgery	2
Chemo-radiation	14

Table 2

Paired Student's t-test and correlation analysis for 16 primary tumors and metastatic nodes

Parameters	Primary tumor N=16 (mean ±std)	Metastatic node N=16 (mean ±std)	p value	Correlation coefficient ρ (p value)
ADC (10^{-3} mm^2/s)	1.05±0.31	1.10±0.26	0.38	0.66(0.004)*
f	0.30±0.10	0.23±0.08	0.0009*	0.60(0.013)*
D (10^{-3} mm^2/s)	0.49±0.24	0.70±0.25	0.0002*	0.71(0.0018)*
D* (10^{-3} mm^2/s)	45.61±24.12	50.47±26.98	0.41	0.70(0.002)*

ρ- correlation coefficient

* denotes p value<0.05

Table 3

Receiver operating characteristic (ROC) curve analysis

Measures	AUC	Threshold	Sensitivity (%)	Specificity (%)	p value
ADC (10^{-3} mm^2/s)	0.55	1.12	62.5	62.5	0.29
f	0.71	0.22	62.5	75.0	0.008*
D (10^{-3} m^2/s)	0.74	0.80	56.2	93.7	0.003*
D^* (10^{-3} m^2/s)	0.53	43.15	62.5	62.5	0.35
[f , D]	0.76	[0.21,0.35]	62.5	81.2	0.0009*

* indicate that the AUC is statistically greater than 0.5 (p value<0.05)